Nanotechnology Perceptions
ISSN 1660-6795
www.nano-ntp.com

Optimization of Machining Parameters of Basalt Fiber and SiO2 Particles Filled Hybrid Polymer Composites using Response Surface Methodology

R. Nagarathna[1], Arun Kumar[2], K. Ganesh[3], Nagesh N[4]

[1]PG Student, Department of Mechanical Engineering, Kuppam Engineering College, India
[2]Assistant Professor, Department of Mechanical Engineering, Kuppam Engineering College, India
[3]Associate Professor and HOD, Department of Mechanical Engineering, Kuppam Engineering, College, India
[4]Associate Professor, Department of Mechanical Engineering, Kuppam Engineering, College, India

Composite materials are currently widely employed in several technical fields, including the sports, chemical, and satellite sectors. The development and use of hybrid polymer composites is expanding across several technical domains. The reinforcement, the matrix, and the processing technique all have a big impact on how machinable the hybrid composite is. Understanding the machining behavior of a certain filled hybrid composite is therefore essential. The main variables influencing the machinability indicators during the dry drilling of novel hybrid composites are examined in this work. These hybrid composites are composed of epoxy reinforced with varying weight proportions of SiO2 particles and basalt fibers: Samples S1, S2, and S4 include 10wt% basalt fiber and 0wt% SiO2, 10 wt% basalt fiber and 2wt% SiO2, 10wt% basalt fiber and 4wt% SiO2, and 10wt% basalt fiber and 6wt% SiO2. Spindle speed, feed rate, drill diameter, and SiO2 weight content were among the drilling parameters optimized in this work using the Box-Benkhen Design of Response Surface Methodology (RSM). With a drop of 24%, the hybrid composites with 1.0 weight percent SiO2 showed the most notable decrease in the delamination factor. With a spindle speed of 1350 rpm, a feed rate of 0.1 mm/rev, a drill diameter of 6 mm, and the addition of 1.0 weight percent SiO2, the lowest delamination factor ever measured was 1.29. The delamination factor decreased even further when the spindle speed was increased. The surface was comparatively smooth, as shown by the observed surface roughness of 1.213 μm. It was clear that increasing the drill diameter and feed

rate increased the surface roughness and delamination factor. The outcomes demonstrated the high projected accuracy of predictive models.
Keywords: machinability, hybrid composite; surface roughess, natural reinforcements.

1. Introduction

A composite is made up of two or more components that work together to produce better results and higher performance metrics than either material alone. In essence, the components were separated into two categories: matrix and reinforcements. The reinforcing phase is much tougher than the matrix phase because it serves as the foundation for composite materials. Composite materials made of polymers are less able to withstand heat and cannot be used in ordinary thermal applications. The several researchers have been side tracked from enhancing the thermal characteristics of the polymer composite. Therefore, a variety of filler materials are employed to improve the mechanical and thermal qualities. Composite materials are employed in a variety of industries, including the automotive and aerospace sectors, because of their superior qualities, which include high strength, stiffness, and decreased weight. Therefore, the material must be machined at different stages.

The first step toward sustainable composite materials are natural fiber reinforced polymer composites, which can also be fully biodegradable when combined with biopolymers [1–3]. They might come from natural sources like basalt, asbestos, and ceramics, or from plant-based sources like jute, hemp, flax, cotton, etc., or animal leftovers like wool, bone, and silk [4]. An volcanic rock called basalt has qualities similar to those of artificial reinforcing materials, however it is more environmentally friendly and natural [5]. Basalt fibers are readily accessible, produced using Junker's technique [6], and used in the petrochemical sector [7], home insulation, car braking, and construction. Basalt fibers are stronger than E-glass, have superior thermal qualities than glass fiber [8], and are more resistant to chemicals than the majority of synthetic fibers.

Additionally, published studies show that basalt fibers are wettable with a variety of polymer resins and that adding them to a polymer composite improves the composite's mechanical qualities [9].

In an attempt to enhance the mechanical performance of basalt fiber reinforced polymer composites, nanofillers have been employed. Carbon nanotubes (CNTs), zinc oxide (ZnO), titanium dioxide (TiO2), nanoclay, titanium carbide (TiC), silicon carbide (SiC), graphene, and other nanofillers have all been tested for this purpose [10–12]. There are three crystalline forms of titanium dioxide, commonly known as titaniumia (TiO2), a white oxide ceramic: rutile, which has a tetragonal structure, anatase, which also has a tetragonal structure, and brookite, which has an orthorhombic structure.It is widely used as Titanium White for white coloring in sensors and the solar sector [13], as well as in paints, inks, and plastics (T. Wang et al., 2022). TiO2 is a non-toxic ananofiller with high optical and electrical qualities, photocatalytic capabilities, and biocompatibility [14–15].

Nanofillers have also been used to reinforce the composite system in basalt fiber epoxy composite materials (BFECs) [16–19]. Additionally, TiO2 has been tested as a coupling agent

with basalt fibers. The fibers' mechanical qualities and resistance to corrosion are improved by the inclusion of TiO2. TiO2 nanoparticle addition in basalt-polysiloxane composites has been investigated with compositions ranging from 0 weight percent to 3 weight percent [20]. The manufactured composite's ideal composition was determined to be 1.5 weight percent TiO2.

Next, considering the strengths of various drill bits, a new tool was created especially for drilling CFRP. The quality of the resulting drilling was then contrasted with other drills. According to a recent study, hole damage may be successfully reduced by using a two end restrict cutting model. They designed their experiment using the ANOVA approach. According to a research, the ideal circumstances for induced delamination have been determined by analyzing the drilling process characteristics. According to [21], the feed rate is a key factor that can cause delamination damage, which is followed by weight percentages of MWCNTs and resisting force. They discovered that the machining efficiency of nano-composites is significantly increased by the addition of MWCNTs. It was noted that the results demonstrated a considerable reduction in delamination damage when loading a tiny quantity of MWCNTs. [22] examined the effects of drilling settings and varying percentages of graphene nanoplatelets on induced delamination damage in composites. Careful testing revealed that modifying a few factors can significantly improve the composites' machining capabilities.

The goal of the current work is to create an environmentally friendly composite material with exceptional qualities using polymers. Since epoxy resin is one of the most used thermoset resins for creating polymer composites in a variety of technical applications, it is chosen as the matrix material [23]. According to published research, TiO2 and SiO2 nanoparticles can be applied to the surface of basalt fibers as coupling agents or for surface treatment. Furthermore, as far as the authors are aware, no research has been done on SiO2 nanoparticles reinforced with basalt fibers in an epoxy matrix. Therefore, the current study focuses on creating composite laminates using natural basalt fibers and environmentally benign SiO2 nanoparticles. The epoxy resin is modified with SiO2 nanoparticles, and the impact of this alteration on the composite laminate's machining and mechanical properties is investigated.

2. Materials and methodology

Materials

The composites were made from plain woven basalt cloth that had an area density of 300 gsm and a density of 2.6 g/cc. As matrix materials, epoxy-Bisphenol A-epichlorohydrin (MY 740) and cyclo-aliphatic amine (HY 951) (room temperature curing procedure) were used. The resin is a transparent liquid with a density of 1.15–1.20 g/cc and a viscosity of 10,000–14,500 mPa.s at 250 °C. The corresponding liquid hardener is said to have a viscosity of 50 to 80 mPa s and a specific gravity of 1.59. Silicon dioxide (SiO2), a nanofiller with a density of 4.26 g/cc and a size range of 30 to 50 nm, was used in this work. In India, it was acquired from Merck.

Fabrication of composite laminates

Composite laminates of basalt fiber-reinforced epoxy with SiO2 nanoparticles (BET) were made by hand lay-up techniques and compression molding. The laminates were made by

changing the weight proportion of SiO2 nanoparticles in the matrix. Table 1 describes the composition and identification of the six produced composite panels, each of which has dimensions of 150 mm by 150 mm by 3 mm. A control panel had epoxy and 0 weight percent SiO2 nanoparticles, whereas the other three composite panels had epoxy-modified nanoparticle weight contents ranging from 2, 4, and 6 weight percent. This particular range of weight percentage addition of SiO2 nanofiller was selected based on the literature review.

Table 1. Composition of the fabricated composites

Sample	Basalt Fibre (wt%)	Epoxy (wt%)	SiO2 (wt%)
S1	10	90	0
S2	10	88	2
S3	10	86	4
S4	10	84	6

In order to create a 3-mm-thick panel, composites were made utilizing basalt fiber in the shape of 150 mm × 150 mm rectangles. After weighing these layers, the same amount of epoxy resin was made. Given the high surface energy of nanoparticles, it was crucial to first establish appropriate separation and guarantee homogeneous particle dispersion in the resin [24]. Nanoparticle agglomeration in the resin would cause incorrect dispersion, which would lead to erroneous findings from the manufactured panels. In order to do this, a magnetic stirrer was used to mix a determined quantity of SiO2 nanoparticles with acetone at room temperature in a 1:10 ratio.

Since acetone is an organic solvent, its presence helps to lower surface energy, which permits particle separation. The use of acetone also lowers the resin's viscosity [25], which makes it possible to create a uniformly changed resin. After sonicating the acetone-nanoparticle combination, the necessary quantity of epoxy was added. Sonication and room temperature stirring were repeated. The mixture was heated to 70 °C and magnetically agitated to eliminate the additional acetone until only epoxy and SiO2 particles were left. Before being utilized for manufacturing, the epoxy was given time to cool. The composite laminates were then manually laid up after this phase. A wooden spatula or stick was used to mix the cooled resin for a minute after adding a matching amount of hardener in a 10:1 (resin-to-hardener) ratio. A compression molding machine with 3 mm spacers was used to cure the wet laid-up panels under pressure [26]. To measure the impact of the SiO2 alteration, a comparative panel made of epoxy and basalt fiber was also constructed. After a week of further hardening, the cured panels were labeled according to Table 1's designation. In order to cut and test them, they were also cleaned.

Testing of mechanical properties of composite laminates

In accordance with ASTM guidelines, testing were conducted on the composite laminates to assess their mechanical qualities. Abrasive water jet machining (AWJM) was used to cut samples from the manufactured panels in order to determine each panel's tensile and flexural strengths. At room temperature, three test specimens were examined for every failure scenario. Table 2 lists specimen sizes based on the following criteria as well as cross-head speeds. After cleaning, the specimens were labeled for examination. A 50 kN capacity universal testing equipment made by INSTRON was used for tensile and flexural testing. To guarantee that the

specimens were positioned correctly for each test, a pre-load of 1N was given to each specimen.

Table 2. Specimen dimensions and test parameters

Mechanical Test	Specimen Dimension (l x b)	Cross-head speed
Tensile Strength	150 mm x 15mm	2 mm/min
Flexural Strength	150 mm x 12.7 mm	1 mm/min

Experimental procedure and design for drilling of composites

The produced hybrid composites used in the experiment have dimensions of 100 mm × 100 mm x 3 mm. A CNC vertical milling machine type YCM-EV1020A was used for the experiment. This machine has a 10 kW spindle and a Fanuc control system. The machining variables and their corresponding levels are shown in Table 3. Table 4 contains the experimental outcomes. The goal of this study's 29 trials is to provide a mathematical formula for analyzing surface roughness and induced delamination damage in holes. For the basalt/SiO2 epoxy hybrid composite, different drill bit sizes were used for every specimen. The cutting instruments were the HSS drill bits. The holes were drilled in accordance with the experiment design. In order to ensure a cleanenvironment and improve the precision of drilled holes incomposites, regular cleaning of the drilling zone on the CNCdrilling machine was carried out using a dust extraction device.

A non-destructive approach was used to evaluate the failuresaround the drilled surface using an image-developingtechnique. The digital images were captured to assess thedamage surrounding the hole. The evaluation was doneusing the publicly available ImageJ 1.50 program.

Delamination and determination of delamination factor (Fd)

When drilling composites, damage from delamination is a serious problem. An evaluation of the damage seen at the drilled hole was done. As shown in Eq. (1), the greatest diameter at the impacted region and the diameter of the drilled hole were measured in order to determine the drilling damage.

$$F_d = D_{max}/D \quad (1)$$

Measurement of surface roughness (Ra)

America Corp. manufactures the MitutoyoSJ-410 kind of surface roughness tester. The measurements were carried out according to a specified protocol and with certain parameters. Four measurements were taken in different areas.

Table 3 displays the drilling parameters and the corresponding levelsthat were utilized

Symbol	Parameters	-1	0	+1
V	Spindle Speed (rpm)	700	1350	2000
F	Feed Rate (mm/rev)	0.1	0.3	0.5
D	Drill diameter (mm)	6	8	10
W	SiO2 content (%)	2	4	6

3. Results and Discussions

Mechanical Properties

Table 4 Mechanical Properties of the Basalt fiber SiO_2 filled hybrid composites

Sample designation	Flexural strength (MPa)	Flexural Modulus (MPa)	Tensile Strength (MPa)
S1	330	14120	250
S2	371	14920	288
S3	399	15870	310
S4	405	16110	308

Table 4 displays the findings of an experimental evaluation of the laminates' behavior under strain. All of the SiO2-filled laminates had improved tensile strength when compared to the empty laminate. Table 4 lists the composite laminates' flexural strength and modulus values. When compared to laminates with 0 weight percent SiO2 nanofiller, the hybridized laminates' flexural strength and modulus have significantly improved as a result of the hybridization produced by adding SiO2 nanofillers to the basalt-reinforced epoxy composites. Additionally, Table 5 makes it evident that the final strength and modulus values of the composite laminates are significantly influenced by the weight percentage loading of the nanofiller.

When SiO2 nanofiller is added up to 6 weight percent, the strength and modulus of the SiO2-filled laminates subjected to bending stresses increase. Across four samples, S1 through S4, the given table shows a steady pattern of improvement in a composite material's mechanical characteristics. It is noteworthy that both flexural strength and flexural modulus show a consistent upward trend, with the former growing from 330 in S1 to 405 in S4 and the latter from 14120 to 16110 throughout the same span.

Tensile strength also exhibits improvement, rising from 250 in S1 to 308 in S4. A systematic optimization of the material's composition or processing is shown by this progressive increase in all three metrics—flexural strength, flexural modulus, and tensile strength—which suggests a significant association between these qualities and the adjustments made.

When a fiber-reinforced laminate is exposed to external loads, matrix splitting causes first fractures. After then, the fractures continue to spread until they reach the area created by the contact between the fiber and matrix. When the fractures approach the interface, they may stop, deflect, or continue to expand until the laminate collapses because of fiber pull-out or fiber fracture [27]. Cracks that emerge in the matrix of an evenly filled fiber-reinforced laminate typically run into the fillers. The energy is absorbed by these fillers, which causes several microcracks to form. These microcracks eventually come into contact with the fibers after continuing to expand.

According to the authors of [28], the presence of uniformly dispersed ZnO nanoparticles within the epoxy matrix led to the creation of microcracks, which ultimately improved the mechanical properties of the polymer composite laminate [29]. This microcrack formation enables the material to absorb more energy. Therefore, compared to unfilled laminates, filled fiber composite laminates often have a higher tensile strength. The homogeneous dispersion of the filler inside the matrix and the uniform coating of the filled resin over the fiber surface, which will provide a strong interface, are two elements that determine the percentage increase

in the tensile strength value of the filled laminates over the unfilled laminates.

Additionally, it is crucial to make sure that the SiO2-filled epoxy resin is evenly applied to all of the fiber surfaces in order to provide a strong interface and almost isotropic behavior. It is difficult to achieve this state when fillers are used. The SiO2 particles have a higher Vander Walls force of attraction and are more likely to form agglomerated clusters because of their larger surface area. These clusters are often dispersed randomly throughout the resin, leaving the fibers without a consistent SiO2 filler layer. This leads to the development of weak interfaces, which ultimately impair the laminate's capacity to support the applied loads.

Table 5 Experiment designmatrix, experimental resultsfor delamination and surfaceroughness

Run	Spindle Speed (V)	Feed rate (F)	Drill Dia (D)	Filler content (%)	Delamination Factor (Fd)	Surface Roughness (Ra)
1	1350	0.1	8	2	1.32	3.7
2	1350	0.3	8	4	1.52	3.4
3	1350	0.3	6	2	1.41	3.5
4	1350	0.3	10	6	1.49	2.9
5	700	0.5	8	4	1.55	4.4
6	700	0.3	10	4	1.68	3.7
7	2000	0.3	6	4	1.28	2
8	1350	0.5	8	6	1.66	3.5
9	700	0.3	8	2	1.55	4.2
10	2000	0.5	8	4	1.59	3.4
11	700	0.3	6	4	1.32	2.5
12	1350	0.1	8	6	1.26	1.9
13	1350	0.3	8	4	1.55	3.6
14	700	0.1	8	4	1.4	3.4
15	1350	0.3	10	2	1.7	4.5
16	1350	0.3	8	4	1.6	3.7
17	700	0.3	8	6	1.4	2.9
18	2000	0.1	8	4	1.41	3.3
19	2000	0.3	8	6	1.41	2.5
20	1350	0.3	8	4	1.65	3.6
21	1350	0.3	6	6	1.42	1.9
22	2000	0.3	8	2	1.45	4.2
23	1350	0.5	8	2	1.65	3.6
24	1350	0.1	10	4	1.52	3.7
25	2000	0.3	10	4	1.45	3.5
26	1350	0.5	6	4	1.48	2.8

27	1350	0.1	6	4	1.35	1.9
28	1350	0.3	8	4	1.72	3.8
29	1350	0.5	10	4	1.8	3.9

Mathematical formulation of drillingparameters using RSM

RSM regression analysis was used to find the coefficient values. The established mathematical model for forecasting surface roughness and the consistent delamination factor is described in Eqs. (2) and (3).

Regression Equation in Uncoded Units

Delamination Factor (Fd) = -0.263 + 0.000672 Spindle Speed (V) - 0.631 Feed rate (F)+ 0.255 Drill Dia (D) + 0.1029 Filler content (%) - 0.000000 Spindle Speed (V)*Spindle Speed (V) - 0.133 Feed rate (F)*Feed rate (F) - 0.00758 Drill Dia (D)*Drill Dia (D) - 0.00977 Filler content (%)*Filler content (%) + 0.000058 Spindle Speed (V)*Feed rate (F) - 0.000037 Spindle Speed (V)*Drill Dia (D) + 0.000021 Spindle Speed (V)*Filler content (%) + 0.0938 Feed rate (F)*Drill Dia (D) + 0.1125 Feed rate (F)*Filler content (%) - 0.01375 Drill Dia (D)*Filler content (%) (2)

Surface Roughness (Ra)= -6.18 + 0.00041 Spindle Speed (V) + 4.84 Feed rate (F) + 2.177 Drill Dia (D) - 0.274 Filler content (%) - 0.000000 Spindle Speed (V)*Spindle Speed (V) - 2.85 Feed rate (F)*Feed rate (F) - 0.1129 Drill Dia (D)*Drill Dia (D) - 0.0348 Filler content (%)*Filler content (%) - 0.00173 Spindle Speed (V)*Feed rate (F) + 0.000058 Spindle Speed (V)*Drill Dia (D) - 0.000077 Spindle Speed (V)*Filler content (%) - 0.438 Feed rate (F)*Drill Dia (D) + 1.063 Feed rate (F)*Filler content (%) + 0.0000 Drill Dia (D)*Filler content (%) (3)

The ANOVA result for the delamination factor is shown in Table 6. The model successfully predicts the response variable, according to this analysis of variance, with a very significant overall effect that is mostly driven by linear connections. Interestingly, the most important variables are drill diameter and feed rate, which show significant linear relationships with the reaction. Although to a lesser degree, filler information also has a substantial linear influence. The squared term of spindle speed shows a substantial quadratic connection, indicating a curved influence, although the linear effect is not statistically significant.

The lack-of-fit test proves that the model well depicts the data and shows that feed rate, drill diameter, and filler content are the main determinants of the response variable. Interaction effects between the parameters are negligible. The impacts of "Feed rate (F)," "Drill Dia (D)," and "Filler content (%)" are very significant (P-value = 0 or 0.017), according to the "Linear" section. This indicates that the response variable is directly and linearly impacted by changes in these parameters. The two most important elements are feed rate and drill diameter, both of which exhibit extremely high F values. With a P-value of 0.148, "Spindle Speed (V)" is not statistically significant at the widely accepted alpha level of 0.05.

This implies that the observed response is less directly impacted by spindle speed in a linear fashion. None of the two-way interactions between the components are statistically significant, according to the "2-Way Interaction" section (P-values > 0.05). This implies that rather than being synergistic, the combined impacts of these elements are mostly additive. "Spindle Speed

(V)*Spindle Speed (V)" has a substantial influence, as demonstrated by the "Square" section (P-value = 0.003). This suggests that there is a quadratic (curved) rather than linear relationship between spindle speed and the response variable.

Table 6 An ANOVA table ispresented for the quadraticmodel of delamination (Fd)

Source	DF	Adj SS	Adj MS	F-Value	P-Value
Model	14	0.433608	0.030972	9.08	0
Linear	4	0.34605	0.086513	25.35	0
Spindle Speed (V)	1	0.008008	0.008008	2.35	0.148
Feed rate (F)	1	0.154133	0.154133	45.16	0
Drill Dia (D)	1	0.1587	0.1587	46.5	0
Filler content (%)	1	0.025208	0.025208	7.39	0.017
Square	4	0.049458	0.012364	3.62	0.032
Spindle Speed (V)*Spindle Speed (V)	1	0.043173	0.043173	12.65	0.003
Feed rate (F)*Feed rate (F)	1	0.000185	0.000185	0.05	0.82
Drill Dia (D)*Drill Dia (D)	1	0.005968	0.005968	1.75	0.207
Filler content (%)*Filler content (%)	1	0.009908	0.009908	2.9	0.11
2-Way Interaction	6	0.0381	0.00635	1.86	0.159
Spindle Speed (V)*Feed rate (F)	1	0.000225	0.000225	0.07	0.801
Spindle Speed (V)*Drill Dia (D)	1	0.009025	0.009025	2.64	0.126
Spindle Speed (V)*Filler content (%)	1	0.003025	0.003025	0.89	0.362
Feed rate (F)*Drill Dia (D)	1	0.005625	0.005625	1.65	0.22
Feed rate (F)*Filler content (%)	1	0.0081	0.0081	2.37	0.146
Drill Dia (D)*Filler content (%)	1	0.0121	0.0121	3.55	0.081
Error	14	0.047778	0.003413		
Lack-of-Fit	10	0.032858	0.003286	0.88	0.606
Pure Error	4	0.01492	0.00373		
Total	28	0.481386			

The surface roughness ANOVA result is shown in Table 7. The ANOVA findings show a highly significant model, showing that the response variable is influenced by Spindle Speed, Feed Rate, Drill Diameter, and Filler Content all together. Interestingly, the biggest linear impacts are shown in Drill Diameter and Filler Content. A non-linear impact is also indicated by the large quadratic connection for Drill Diameter. There is a considerable interaction between Feed Rate and Filler Content, although overall interaction effects are negligible. Although the near-significant Lack-of-Fit indicates the need for more modification to capture remaining changes, the model is largely appropriate.

The "Model" row displays a P-value of 0 and an extremely high F-value of 13.44. This suggests that the components included in the model are successfully explaining the variation in the response, and the model as a whole is highly statistically significant. The "Linear" section

demonstrates that all four factors—Spindle Speed (V), Feed Rate (F), Drill Diameter (D), and Filler Content (%)—have statistically significant linear effects (P-values < 0.05). The most significant linear factors are Drill Diameter (D) and Filler Content (%), which both exhibit exceptionally high F-values (63.34 and 71.95, respectively). A P value of 0.002 indicates that feed rate also has a significant impact. The influence of spindle speed is less pronounced but still noteworthy.

A strong quadratic association between drill diameter and reaction is indicated by the extremely significant P-value (0.001) of "Drill Dia (D)*Drill Dia (D)". The "Feed rate (F)*Filler content (%)" has a significant p value of 0.008, whereas the "2-Way Interaction" section has a marginal P-value of 0.08. This demonstrates that there is a discernible impact on the reaction from the relationship between feed rate and filler material. The other exchanges don't.

Table 7 Presents the Analysisof Variance (ANOVA) fora quadratic model-surfaceroughness (Ra)

Source	DF	Adj SS	Adj MS	F-Value	P-Value
Model	14	14.2948	1.02106	13.44	0
Linear	4	11.825	2.95625	38.9	0
Spindle Speed (V)	1	0.4033	0.40333	5.31	0.037
Feed rate (F)	1	1.1408	1.14083	15.01	0.002
Drill Dia (D)	1	4.8133	4.81333	63.34	0
Filler content (%)	1	5.4675	5.4675	71.95	0
Square	4	1.3598	0.33995	4.47	0.015
Spindle Speed (V)*Spindle Speed (V)	1	0.0173	0.01732	0.23	0.64
Feed rate (F)*Feed rate (F)	1	0.0845	0.08455	1.11	0.309
Drill Dia (D)*Drill Dia (D)	1	1.3233	1.32326	17.41	0.001
Filler content (%)*Filler content (%)	1	0.1256	0.12563	1.65	0.219
2-Way Interaction	6	1.11	0.185	2.43	0.08
Spindle Speed (V)*Feed rate (F)	1	0.2025	0.2025	2.66	0.125
Spindle Speed (V)*Drill Dia (D)	1	0.0225	0.0225	0.3	0.595
Spindle Speed (V)*Filler content (%)	1	0.04	0.04	0.53	0.48
Feed rate (F)*Drill Dia (D)	1	0.1225	0.1225	1.61	0.225
Feed rate (F)*Filler content (%)	1	0.7225	0.7225	9.51	0.008
Drill Dia (D)*Filler content (%)	1	0	0	0	1
Error	14	1.0638	0.07599		
Lack-of-Fit	10	0.9758	0.09758	4.44	0.082
Pure Error	4	0.088	0.022		
Total	28	15.3586			

Optimization of the responses

As seen in Fig. 1, the optimization plot and the ANOVA results support the importance of the input factors, especially Drill Diameter, Feed Rate, and Filler Content. The plot shows the precise ideal values for these parameters in order to minimize surface roughness and delamination and maximize composite desirability. The Spindle speed has an effect, but it is much less than the other factors. The graph gives a visual representation of how each of these factors affect the output, and how they relate to each other in terms of optimization.

The figure indicates that increased spindle speed, feed rate, drill diameter, and filler content are often desired in order to reduce surface roughness. The figure indicates that a medium spindle speed, a medium drill diameter, a medium filler content, and a greater feed rate are ideal for minimizing delamination. The optimization plot demonstrates that a successful optimization is achieved when all components are adjusted to their ideal values, yielding a Composite Desirability of 1.000. Spindle Speed: 2000.0, Feed Rate: 0.50, Drill Diameter: 10.0, and Filler Content: 6.0 are the precise ideal parameters.

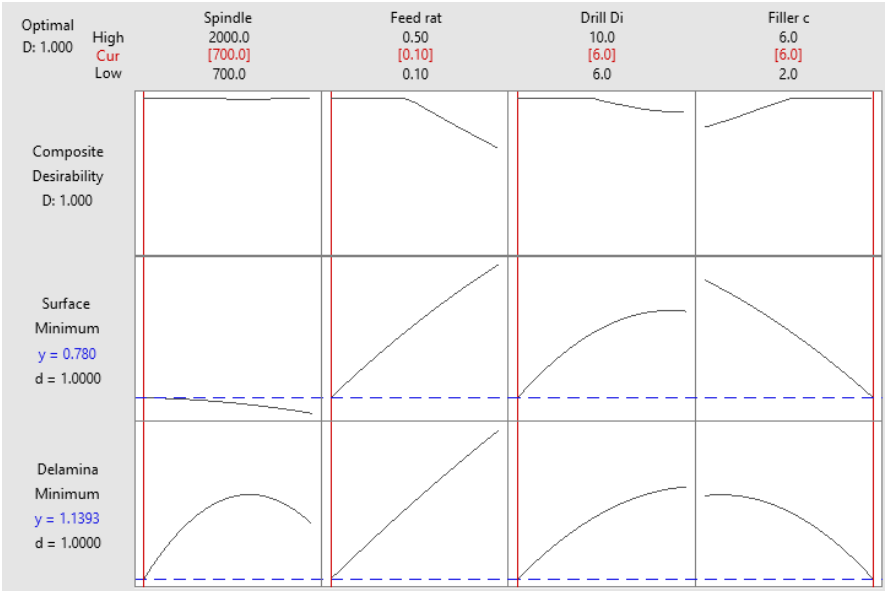

Fig. 1 Optimization plot of the responses

Contour plots analysis of responses

With spindle speed and drill diameter maintained constant, this contour map shows how feed rate and filler content impact surface roughness. Regardless of the filler content, increasing the feed rate dramatically lowers surface roughness. The effect of filler content is negligible, particularly at lower feed rates. Low filler content and high feed rates result in the lowest Surface Roughness. Higher feed rates (about 0.4 to 0.5) and lower filler content values (around 2% to 4%) result in the lightest green zone, which indicates the lowest surface roughness (Ra < 2.0). In the investigated ranges, feed rate has a greater effect on surface roughness than filler content.

Surface roughness is regularly decreased by increasing the feed rate. Feed rate and filler

content seem to have a small interaction impact. At lower feed rates, the impact of filler content on surface roughness is more apparent.

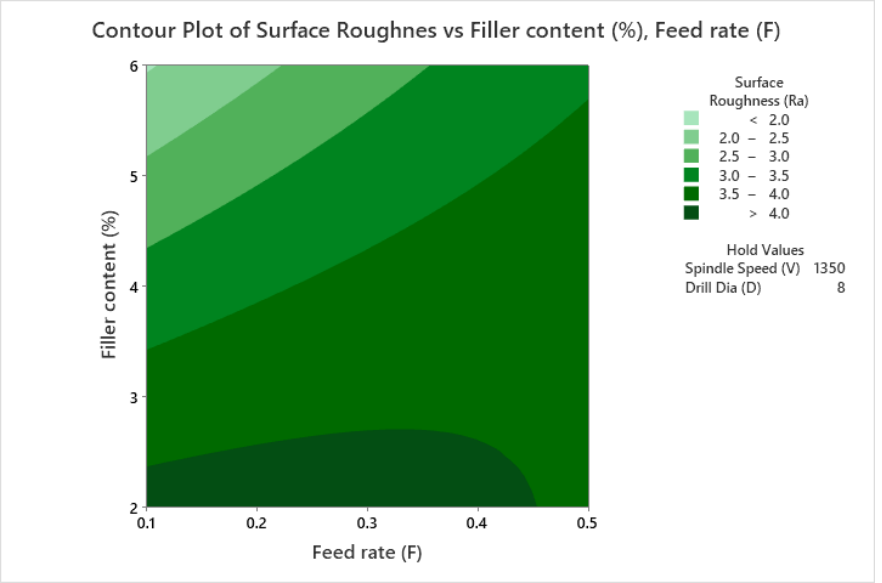

Fig. 2 Contour plot of surface roughness

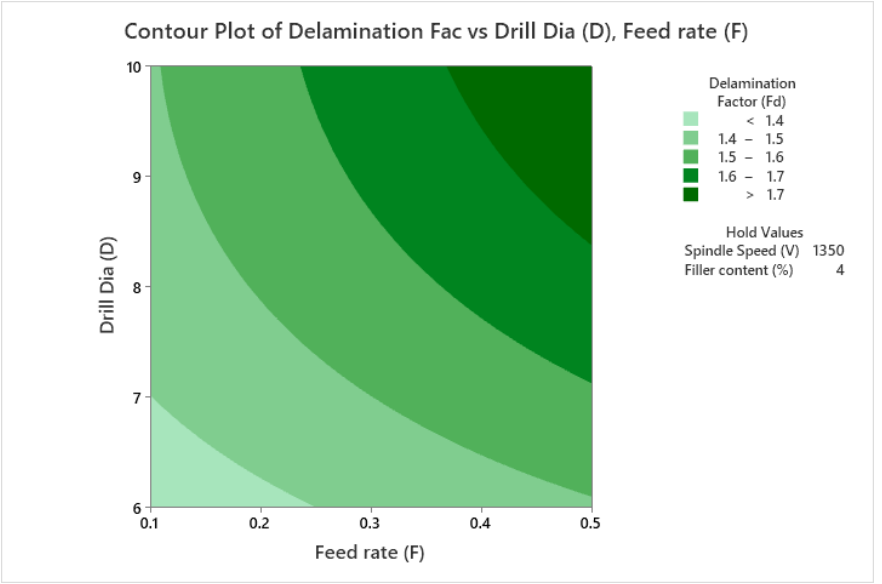

Fig. 3 Contour plot of delamination

With Spindle Speed and Filler Content maintained constant, this contour map illustrates the relationship between Drill Diameter and Feed Rate and Delamination Factor. Delamination is reduced via smaller drill diameters and lower feed rates. On the other hand, more delamination results from bigger drill diameters and higher feed rates. In order to attain the best outcomes,

these parameters must be carefully controlled because they are directly and favorably correlated with delamination. Lower feed rates (about 0.1 to 0.2) and drill diameters (about 6 to 7) result in the lightest green zone, which indicates the lowest delamination factor (Fd< 1.4). The delamination factor (darker green) rises in tandem with the feed rate. This pattern holds true for all drill diameters. The delamination factor (darker green) rises in tandem with the drill diameter.

This pattern holds true at all feed rates. Higher feed rates (about 0.4 to 0.5) and drill diameters (about 9 to 10) are associated with the darkest green zone, which indicates the largest delamination factor (Fd> 1.7). The delamination factor is directly positively correlated with both drill diameter and feed rate. The delamination factor deteriorates as one of these factors rises. While maintaining the Spindle Speed at 1350 and the Filler Content at 4, it is advised to utilize lower feed rates and drill diameters to reduce delamination. To reduce delamination in a production context, it is essential to regulate both the drill diameter and the feed rate. Better delamination results will be obtained by using lower values for both factors.

4. Conclusion

Flexural strength and flexural modulus clearly improve when the sample designation moves from S1 to S4, according to the data. Additionally, tensile strength first rises while S4 somewhat declines. First, the material itself was optimized, leading to a peak tensile strength of 310 MPa and enhanced modulus and flexural strength (from 14120 to 16110 MPa and 330 to 405 MPa, respectively). The machinability illustrates how changes in Spindle Speed, Feed Rate, Drill Diameter, and Filler Content affect Surface Roughness (Ra) and Delamination Factor (Fd). The significance of carefully choosing machining parameters to achieve the desired surface smoothness and reduce delamination is shown by the process parameter optimization (Runs 1–29).

The two most important variables affecting surface roughness and delamination are feed rate and drill diameter. When spindle speed is 1350 and filler content is 4%, the drilling process was adjusted to reveal that smaller drill diameters (about 6-7) and lower feed rates (approximately 0.1-0.2) are essential for minimizing delamination (Fd). Higher feed rates are necessary to minimize surface roughness (Ra), which is in contradiction with this.

References

1. Rastogi, S., Verma, A., & Singh, V. K. (2020). Experimental response of nonwoven waste cellulose fabric–reinforced epoxy composites for high toughness and coating applications. Materials Performance and Characterization, 9(1), 151–172.
2. , Verma, A., & Singh, V. K. (2019). Dynamic mechanical analysis and creep-recovery behaviour of polyvinyl alcohol based cross-linked biocomposite reinforced with basalt fiber. Materials Research Express, 6(10), 105373.
3. Weyhrich, C. W., Petrova, S. P., Edgar, K. J., & Long, T. E. (2023). Renewed interest in biopolymer composites: Incorporation of renewable, plant-sourced fibers. Green Chemistry: An International Journal and Green Chemistry Resource: GC, 25(1), 106–129.
4. Gholampour, A., & Ozbakkaloglu, T. (2020). A review of natural fiber composites: Properties, modification and processing techniques, characterization, applications. Journal of Materials

Science, 55(3), 829–892.
5. Afolabi, L. O., et al. (2020). Syntactic foams formulations, production techniques, and industry applications: A review. Journal of Materials Research and Technology, 9(5), 10698–10718.
6. Tamás-Bényei, P., & Sántha, P. (2023). Potential applications of basalt fibre composites in thermal shielding. Journal of Thermal Analysis and Calorimetry, 148(2), 271–279.
7. Chowdhury, I. R., Pemberton, R., & Summerscales, J. (2022). Developments and industrial applications of basalt fibre reinforced composite materials. Journal of Composites Science, 6(12), 367.
8. Xing, D., et al. (2023). Thermoelectric performance of basalt fiber with nanocomposite sizing. Colloids and Surfaces A Physicochemical and Engineering Aspects, 672, 131761.
9. Jain, N., Verma, A., & Singh, V. K. (2019). Dynamic mechanical analysis and creep-recovery behaviour of polyvinyl alcohol based cross-linked biocomposite reinforced with basalt fiber. Materials Research Express, 6(10), 105373.
10. Mohit, H., et al. (2021). Nanoparticles addition in CoirBasalt-Innegra fibers reinforced Bio-synthetic epoxy composites. Journal of Polymers and the Environment, 29(11), 3561–3573.
11. Othman, F. E. C., & Hassan, S. A. (2023). Hybrid biocomposites combining synthetic nanofillers and natural fibers in composite structures. Synthetic Natural Nanofillers Polymer Composite, 259–272.
12. Sharma, K. K., Kushwaha, J., Kumar, K., Singh, H., & Shrivastava, Y. (2022). Fabrication and testing of hybrid fibre reinforced composite: A comprehensive review. Australian Journal of Mechanical Engineering, 1–17.
13. Nunzi, F., & De Angelis, F. (2022). Modeling titanium dioxide nanostructures for photocatalysis and photovoltaics. Chemical Science, 13(33), 9485–9497.
14. Brillas, E., & Garcia-Segura, S. (2023). Recent progress of applied TiO2 photoelectrocatalysis for the degradation of organic pollutants in wastewaters. Journal of Environmental Chemical Engineering, 109635(3), 109635.
15. Tripathy, P., & Biswas, S. (2022a). Mechanical and thermal properties of basalt fiber reinforced epoxy composites modified with CaCO3 nanoparticles. Polymer Composites, 43(11), 7789–7803.
16. Joshi, S., Hiremath, A., Nayak, S. Y., Jaideep, J. P., & Thipperudrappa, S. (2022). Hybridization effect on the mechanical properties of basalt fiber reinforced ZnO Iyer et al., Cogent Engineering (2023), 10: 2227397 https://doi.org/10.1080/23311916.2023.2227397 modified epoxy composites. Polymer Composites, 43 (8), 5704–5714.
17. Kishore, M., Amrita, M., & Kamesh, B. (2021). Tribological properties of basalt-jute hybrid composite with graphene as nanofiller. Materials Today: Proceedings, 43, 244–249.
18. Vinay, S. S., Sanjay, M. R., Siengchin, S., & Venkatesh, C. V. (2022). Basalt fiber reinforced polymer composites filled with nano fillers: A short review. Materials Today: Proceedings, 52, 2460–2466.
19. Zheng, Y., Zhuo, J., & Zhang, P. (2021). A review on durability of nano-SiO2 and basalt fiber modified recycled aggregate concrete. Construction and Building Materials, 304, 124659.
20. Mishra, R., Tiwari, R., Marsalkova, M., Behera, B. K., & Militky, J. (2012). Effect of TiO2 nanoparticles on basalt/polysiloxane composites: Mechanical and thermal characterization. The Journal of the Textile Institute, 103(12), 1361–1368.
21. Kumar, R., Haq, M. I. U., Raina, A., & Anand, A. (2019). Industrial applications of natural fibre-reinforced polymer composites – challenges and opportunities. International Journal of Sustainable Engineering, 12 (3), 212–220.
22. R.K.; Hu, H.; Wambua, P.; Gu, B. Characterizations of basalt unsaturated polyester laminates under static three-point bending and low-velocity impact loadings. Polym. Compos. 2014, 35, 2203–2213.
23. Verma, A., & Singh, V. K. (2019). Dynamic mechanical analysis and creep-recovery behaviour

of polyvinyl alcohol based cross-linked biocomposite reinforced with basalt fiber. Materials Research Express, 6(10), 105373.

24. Shen, J., Lin, X., Liu, J., & Li, X. (2020). Revisiting stress– strain behavior and mechanical reinforcement of polymer nanocomposites from molecular dynamics simulations. Physical Chemistry Chemical Physics: PCCP, 22(29), 16760–16771.
25. Zhang, Y., Chen, M., Gu, M., & Wu, L. (2022). Scalable and waterborne titanium-dioxide-free thermochromic coatings for self-adaptive passive radiative cooling and heating. Cell Reports Physical Science, 3(3), 100782.
26. Nayak, S. Y., et al. (2020). Influence of fabric orientation and compression factor on the mechanical properties of 3D E-glass reinforced epoxy composites. Journal of Materials Research and Technology, 9(4), 8517–8527.
27. Khandelwal, S., & Rhee, K. Y. (2020). Recent advances in basalt-fiber-reinforced composites: Tailoring the fiber-matrix interface. Composites Part B Engineering, 192, 108011.
28. Thipperudrappa, S., Hiremath, A., & Kurki Nagaraj, B. (2021). Synergistic effect of ZnO and TiO2 nanoparticles on the thermal stability and mechanical properties of glass fiber-reinforced LY556 epoxy composites. Polymer Composites, 42(9), 4831–4844.
29. Thipperudrappa, S., Ullal Kini, A., & Hiremath, A. (2019). Influence of zinc oxide nanoparticles on the mechanical and thermal responses of glass fiber-reinforced epoxy nanocomposites. Polymer Composites, 41(1), 174–181.